Pergamon

Int. J. Heat Mass Transfer. Vol. 40, No. 8, pp. 1839–1851, 1997

0017 9310/97 $17.00 + 0.00

PII: S0017-9310(96)00249-9

Numerical analysis of turbulent pipe flow in a transverse magnetic field

H.-C. JI† and R. A. GARDNER

Department of Mechanical Engineering, Washington University, St. Louis, MO 63130, U.S.A.

(*Received* 1 *August* 1995 *and in final form* 27 *June* 1996)

Abstract—The damping of turbulence by a constant transverse magnetic field was explored using the standard k–ε turbulence model modified to account for the direct interaction of the applied field with turbulent fluctuations. The coupled mass, momentum, energy and magnetic induction equations were solved numerically providing an efficient technique for investigating the effects of electromagnetic suppression of turbulence in the flow of an electrically conducting fluid through an electrically insulated pipe with a uniform heat flux at the wall and an applied constant transverse magnetic field. The numerical results qualitatively demonstrated the effects of turbulence suppression by the magnetic field and correctly predicted the mutual antagonism between inertial and magnetic forces. The computed velocity profiles, skin friction, temperature profiles and the Nusselt numbers covered a range of Reynolds numbers from 16 000 to 1 000 000 and Hartmann numbers from 0 to 375, and showed agreement with available experimental data. An empirical equation for the average Nusselt number as a function of the Peclet number and the Hartmann number is presented.

1. INTRODUCTION

Magnetohydrodynamic (MHD) interactions have assumed growing importance in metallurgical applications with the development of techniques using stationary fields to suppress instabilities creating favorable flow conditions in tundish devices as reported by Szekely and Ilegbusi [1]. Time varying fields, on the other hand, have been used to induce mixing during the casting of metals and also to control the growth of semiconductor crystals. A comprehensive collection of examples of the use of magnetic fields in metallurgical applications, energy conversion and other MHD flows can be found in the sixth Beer-Sheva International Seminar on MHD Flows and Turbulence edited by Branover and Unger [2]. In addition, one recent novel application of MHD is the design of superconducting MHD propulsion system as reported by Imaichi [3].

While the first MHD analyses were either analytical laminar flows or experimental investigations, the development of computational techniques and numerical models now allow turbulent MHD interactions to be explored in more detail. See Branover and Unger [4] for recently reported MHD studies or Bradshaw [5] for an overview of a comparison of models for turbulent flows.

This paper focuses on a geometrically simple MHD pipe flow which exhibits the complex interaction between an applied field and turbulence. An electrically conducting fluid flows in a horizontal, electrically insulated pipe under either isothermal conditions or with heat transfer with a constant heat flux at the wall. The applied field interacts with the flow creating a ponderomotive body force which changes the axisymmetric velocity profile to a wedge-shaped profile while simultaneously damping out turbulent fluctuations. With a constant wall heat flux imposed on the flow, the resulting temperature profiles also take on an angular dependence. If the heating rates are high enough to stimulate secondary flow due to natural convection, the field also acts to inhibit the natural convection.

2. EQUATIONS

The flow is governed by a set of coupled partial differential equations that express the conservation of mass, momentum, energy and the interaction of the flow with the magnetic field. Certain simplifying assumptions are listed below.

- The viscous dissipation and Joulean heating are neglected in the energy equation.
- The interaction of the induced axial magnetic field with the flow is considered to be negligible compared to the interaction of the applied magnetic field, B_0, with the flow.
- The pipe wall is assumed to be electrically insulated with a constant heat flux at the boundary.
- The mean flow is fully developed and the applied magnetic field and wall heat flux are uniform and constant in time.
- All fluid properties such as density, specific heat and viscosity are assumed constant.

† Present address: Department of Psychiatry, WUSM, 4559 Scott Avenue G16, St. Louis, MO 63110, U.S.A.

NOMENCLATURE

B	magnetic field [T]
B_0	applied constant magnetic field [T]
B_z	axial magnetic field induction [T]
C	specific heat [J kg^{-1}°C^{-1}]
C_f	skin friction ($\bar{\tau}_w/\frac{1}{2}\rho\bar{v}_z^2$)
C_1, C_2, C_μ	turbulence model constants
d	pipe diameter [m]
$D_m(r,\phi)$	magnetic damping amplification
f_2, f_μ	turbulence damping functions
F_B	buoyancy force [N m^{-3}]
Gr	Grashof number ($g\beta q'' d^4/\nu^2 K$)
j	electric current density [Am^{-2}]
k	turbulent kinetic energy [m^2 s^{-2}]
K	thermal conductivity [W m^{-1}°C^{-1}]
M	Hartmann number ($B_0 R(\sigma/\mu)^{1/2}$)
MHD	magneto-hydro-dynamic
N	interaction parameter ($B_0^2\,\mathrm{d}\sigma/\rho\bar{v}_z$)
Nu	Nusselt number $(-2R/(T_w-T_b)(\mathrm{d}T/\mathrm{d}y)_w)$
$\overline{Nu}$	average Nusselt number $(1/\pi\int_0^\pi Nu\cdot \mathrm{d}\varphi)$
Pe	Peclet number ($Re\cdot Pr$)
Pr	Prandtl number, ($\mu C/K$)
R_T	turbulent Reynolds number ($\rho k^2/\varepsilon\mu$)
q''	wall heat flux [W m^{-2}]
r	radial coordinate [m]
R	radius of pipe [m]
Re	Reynolds number, ($\bar{v}_z d/\nu$)
Re_m	magnetic Reynolds number ($d\bar{v}_z/\eta$)
T	temperature [°C]
T_b	liquid bulk temperature ($\int_A \rho v_z T\,\mathrm{d}A/\int_A \rho v_z\,\mathrm{d}A$)
v_r	radial velocity [m s^{-1}]
v_ϕ	azimuthal velocity [m s^{-1}]
v_z	axial velocity [m s^{-1}]
$\bar{v}_z$	mean axial velocity [m s^{-1}]
y	distance from wall [m]
y^+	log-law coordinate
z	axial direction [m]
δ_H	thickness of Hartmann layer [m]
ε	turbulence dissipation rate [m^2 s^{-3}]
ε_H	eddy diffusivity for heat transfer [m^2 s^{-1}]
ϕ	azimuthal angle
η	magnetic diffusivity [m^2 s^{-1}]
μ	dynamic viscosity [kg m^{-1} s^{-1}]
μ_0	permeability of free space [kg m A^{-2} s^{-2}]
ν	kinematic viscosity [m^2 s^{-1}]
ρ	density [kg m^{-3}]
σ	electrical conductivity [Ω^{-1} m^{-1}]
σ_k, σ_h, σ_ε	turbulence model constants
τ	skin friction [N m^{-2}]
$\bar{\tau}$	average wall shear stress [N m^{-2}].

Subscripts

C	core region
eff	effective
H	Hartmann layer region
t	turbulent
w	wall.

The cylindrical coordinate system for the problem is shown in Fig. 1. The radial coordinate, r, is positive outward from the axis, the polar angle, ϕ, is measured positive clockwise from the vertical and the axial coordinate, z, is positive into the paper.

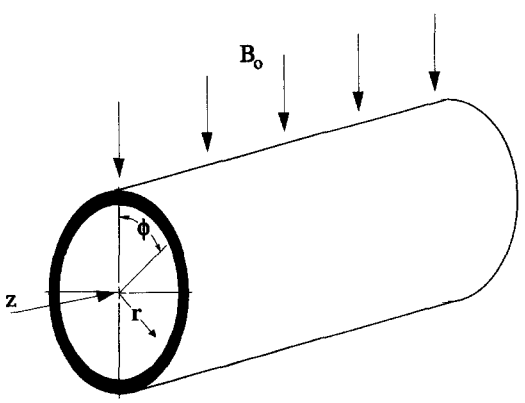

Fig. 1. Coordinate system for turbulent pipe flow with transverse magnetic field.

The corresponding steady-state MHD equations are listed as follows.

- Continuity equation

$$\frac{1}{r}\frac{\partial \rho r v_r}{\partial r}+\frac{1}{r}\frac{\partial \rho v_\phi}{\partial \phi}+\frac{\partial \rho v_z}{\partial z}=0. \tag{1}$$

- Axial momentum equation

$$\rho v_z\frac{\partial v_z}{\partial z}=-\frac{\partial p}{\partial z}+\frac{1}{r}\frac{\partial}{\partial r}\left(r\mu_{\mathrm{eff}}\frac{\partial v_z}{\partial r}\right)$$
$$+\frac{1}{r^2}\left(\frac{\partial}{\partial \phi}\mu_{\mathrm{eff}}\frac{\partial v_z}{\partial \phi}\right)+\frac{B_0}{\mu_0}\left(\frac{\sin\phi}{r}\frac{\partial B_z}{\partial \phi}-\cos\phi\frac{\partial B_z}{\partial r}\right). \tag{2}$$

- Energy equation

$$\rho C v_z\frac{\partial T}{\partial z}=\frac{1}{r}\frac{\partial}{\partial r}\left(rK_{\mathrm{eff}}\frac{\partial T}{\partial r}\right)+\frac{1}{r^2}\frac{\partial}{\partial \phi}\left(K_{\mathrm{eff}}\frac{\partial T}{\partial \phi}\right). \tag{3}$$

Here, T is the local temperature and turbulence is modeled using the eddy viscosity concept which comes from the usual Reynold's-averaging technique applied to the appropriate equations. The effective viscosity is

defined as the sum of molecular viscosity and turbulent viscosity ($\mu_{\text{eff}} = \mu + \mu_t$), and the effective thermal conductivity is modeled as the sum of molecular conductivity and turbulent conductivity ($K_{\text{eff}} = K + K_t$). The values of μ_{eff} and K_{eff} are computed using the k–ε turbulence model.

• Induction equation

$$0 = \frac{1}{r}\frac{\partial}{\partial r}\left(r\eta\frac{\partial B_z}{\partial r}\right) + \frac{1}{r^2}\frac{\partial}{\partial \phi}\left(\eta\frac{\partial B_z}{\partial \phi}\right) + B_0\left(\frac{\sin\phi}{r}\frac{\partial v_z}{\partial \phi} - \cos\phi\frac{\partial v_z}{\partial r}\right). \quad (4)$$

Here the term η is the coefficient of magnetic diffusivity. The coupling between the momentum equation and the induction equation occurs via the ponderomotive force term in equation (2). Ampere's law ($\mu_o \mathbf{j} = \nabla \times \mathbf{B}$) was used to obtain an expression of the ponderomotive force which couples the momentum equation and the magnetic induction, Ferraro and Plumpton [6] and Gold [7]. It should be noted that the axial diffusion terms in the axial momentum equation and the energy equation are absent. The first due to the fact that the flow is fully developed and the second because the heat transfer at the wall is constant causing the temperature gradient in the axial direction to be constant.

The boundary conditions for equations (1) through (4) at $r = R$ are given by

$$v_z = 0, \quad B_z = 0, \quad \text{and} \quad \frac{\partial T}{\partial r} = -\frac{q''}{K} \quad (5)$$

and a condition of symmetry existing at $r = 0$ such that

$$\frac{\partial v_z}{\partial r} = \frac{\partial B_z}{\partial r} = \frac{\partial T}{\partial r} = 0. \quad (6)$$

The important parameters that characterize the interaction of the magnetic field with a turbulent flow are the Hartmann number (M), the Reynolds number (Re) and the interaction parameter (N):

$$M = B_0 d\left(\frac{\sigma}{\mu}\right)^{1/2} \quad Re = \frac{\bar{v}_z d}{\nu} \quad N = \frac{B_0^2 d\sigma}{\rho \bar{v}_z}. \quad (7)$$

The Hartmann number represents the square root of the ratio of the characteristic ponderomotive (electromagnetic) force ($\sigma B_0^2 \bar{v}_z$) to the viscous force ($\mu_0 \bar{v}_z / d^2$), the Reynolds number the usual ratio of the inertia to viscous forces and the interaction parameter the ratio of the ponderomotive force ($\sigma B_0^2 \bar{v}_z$) to the inertia force ($\rho \bar{v}_z^2 / d$). While the interaction parameter is fundamentally involved in the action of the field in damping turbulent fluctuations, it is sufficient to consider only two of the three nondimensional parameters because it is easy to show that $N = M^2/Re$. Here M and Re will be used to describe the flow interactions and N is used in the turbulence model.

3. TURBULENCE AND TURBULENCE MODELING

Turbulence measurements in the literature indicate that the application of a transverse magnetic field to a turbulent pipe flow flattens velocity profiles (the Hartmann effect), damps turbulent fluctuations and reduces heat transfer. The measured velocity profiles for a flow of mercury [8], indicate that the velocity profile changed from an axisymmetric profile to a wedge shaped profile as the field was increased. Turbulent fluctuations were damped first in the central region of the cross section, but eventually all fluctuations could be damped out causing the flow to become laminar flow even if the Reynolds number was several orders of magnitude above the usual transition value of 2300. Patrick [9] mapped the damping of the turbulent fluctuations in a similar horizontal pipe flow with a transverse field and clearly showed that the damping depended on the radial and angular position in the flow as shown in Fig. 2. Measurements of the turbulent power spectrum [8], indicated that turbulent fluctuations were uniformly damped at all frequencies. The skin friction coefficient was first found to decrease due to the damping of the fluctuations and then to increase linearly with the Hartmann number, demonstrating the dominance of the Hartmann effect after the flow had undergone its laminarization.

In terms of heat transfer, a survey of the literature indicates that a stationary magnetic field significantly changes the heat transfer characteristics. Genin, Manchkha and Sviridov [10] found that a longitudinal magnetic field caused a significant reduction of the heat transfer coefficient; Genin, Kovalev and Sviridov [11] observed a similar behavior. Gardner and Lykoudis [12, 13] experimentally investigated the case of a transverse magnetic field in a horizontal pipe and found that a transverse magnetic field reduced the average Nusselt number by as much as 70%. In order to predict heat transfer in a turbulent flow subjected to an applied transverse magnetic field, the fundamental interaction between the magnetic field and turbulence must be understood.

There are currently several turbulence models available in the literature for modeling turbulent channel or pipe flows with applied magnetic fields. Branover [14], Branover and Vasil'ev [15], Branover and Gel'fgat [16], Branover, Gel'fgat and Tsinober [17] proposed mixing length models for smooth and rough-walled channels with either longitudinal or transverse magnetic fields. Lykoudis and Brouillette [18] also applied a mixing length approach to model turbulent channel flow with a transverse magnetic field. No suitable turbulence model has been found in the literature which is capable of modeling the complex radial and azimuthal interactions found in a turbulent pipe flow with a transverse magnetic field.

3.1. *Turbulence model*

Presently, one of the most widely used turbulence models for computing complex flows is the k–ε tur-

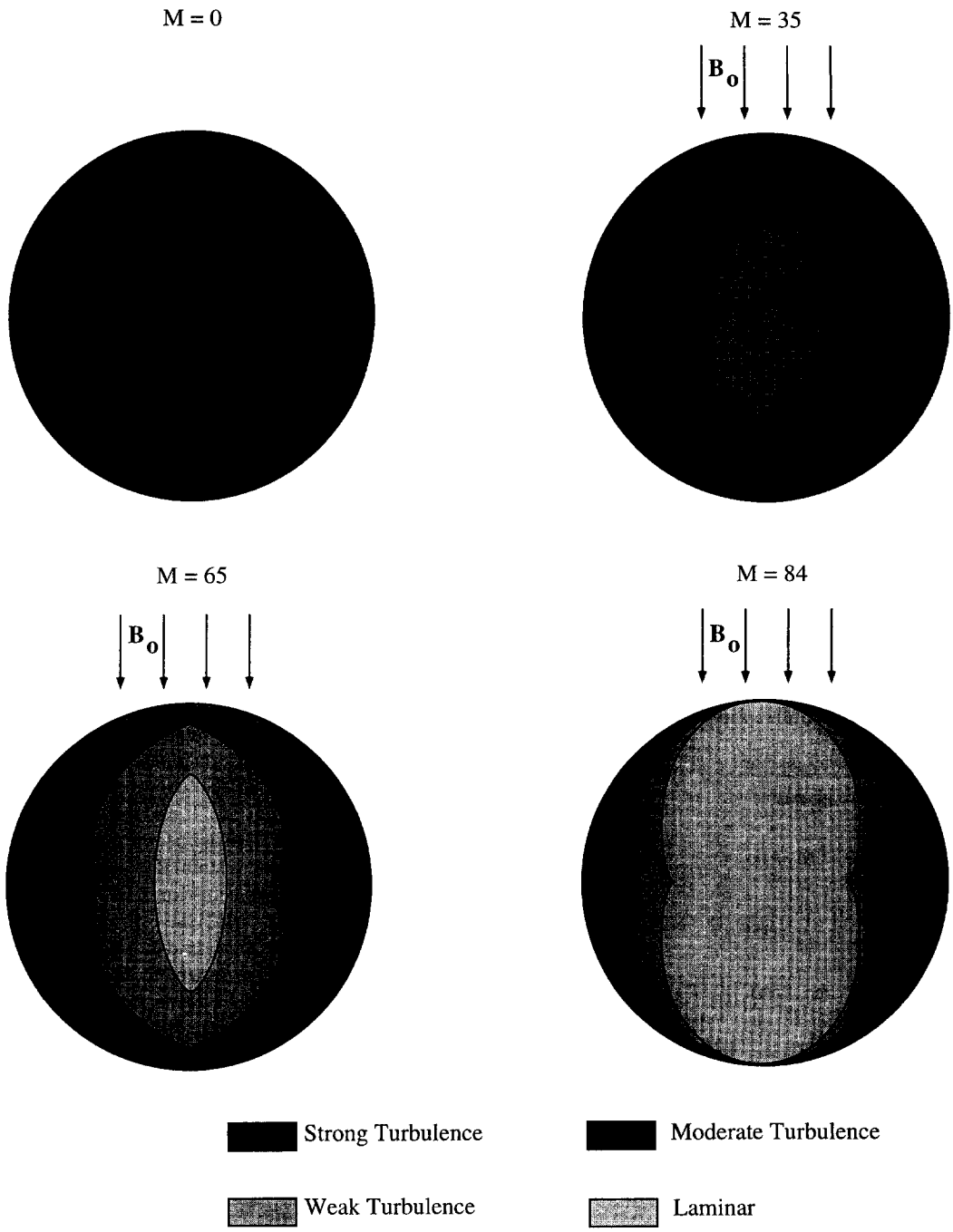

Fig. 2. Qualitative picture of magnetic turbulence suppression for $Re = 50\,000$ [9].

bulence model, Launder *et al.* [19], Jones and Launder [20]. Unfortunately, the k–ε turbulence model contains no term which models the damping of turbulence by the magnetic field. Here, a modification to the k–ε turbulence is proposed which enables the k–ε turbulence model to be used for turbulent flows where the damping action of the magnetic field is significant. The modified k–ε turbulence model will be used to analyze the turbulent flow of an electrically conducting fluid in a horizontal turbulent pipe.

The k–ε turbulence model equations for modeling the turbulent pipe flow with transverse magnetic field are given by the following equations [21]:

- Turbulence kinetic equation

$$\frac{\partial}{\partial z}(\rho v_z k) = \frac{1}{r}\frac{\partial}{\partial r}\left(r\frac{\mu_t}{\sigma_k}\frac{\partial k}{\partial r}\right) + \frac{1}{r^2}\frac{\partial}{\partial \phi}\left(\frac{\mu_t}{\sigma_k}\frac{\partial k}{\partial \phi}\right) + G - \rho\varepsilon - 2\mu\left(\frac{\partial k^{1/2}}{\partial r}\right)^2 - A \cdot D_m(r,\phi)\sigma B_0^2 k\, e^{-BN}. \quad (8)$$

- Turbulence dissipation equation

$$\frac{\partial}{\partial z}(\rho v_z \varepsilon) = \frac{1}{r}\frac{\partial}{\partial r}\left(r\frac{\mu_t}{\sigma_\varepsilon}\frac{\partial \varepsilon}{\partial r}\right) + \frac{1}{r^2}\frac{\partial}{\partial \phi}\left(\frac{\mu_t}{\sigma_\varepsilon}\frac{\partial \varepsilon}{\partial \phi}\right)$$

$$+\frac{C_1 \varepsilon G}{k} - C_2 f_2 \rho \frac{\varepsilon^2}{k} + 2\frac{\mu\mu_t}{\rho}\left(\frac{\partial^2 v_z}{\partial r^2}\right)^2 - A\,\mathrm{e}^{-BN}\sigma B_0^2 k\left(\frac{\varepsilon}{k}\right) \tag{9}$$

where N is the interaction parameter, and A and B are empirical constants which need to be determined from available experimental data. The boundary conditions are $k = \varepsilon = 0$ at the wall and k and ε have zero gradients at $r = 0$ due to the symmetry of the problem.

It should be noted that the additional term $2\mu((\partial k^{1/2}/\partial r))^2$ in the equation (8) is introduced by the originators of the turbulence model for computational rather than physical reasons, Jones and Launder [20]. It was done to allow artificial assignment a value of zero for ε at the wall and to introduce the extra term in the k equation. In addition, the extra term $2\mu\mu_t/\rho(\partial^2 v_z/\partial r^2)^2$ in equation (9) is included in the ε equation to produce satisfactory variation of k with distance from the wall [20].

In equations (8) and (9), the turbulence production G is given by,

$$G = 2\mu_t\left[\left(\frac{\partial v_r}{\partial r}\right)^2 + \left(\frac{1}{r}\frac{\partial v_\phi}{\partial \phi} + \frac{v_r}{r}\right)^2\right] + \mu_t\left[\left(\frac{1}{r}\frac{\partial v_z}{\partial \phi}\right)^2 + \left(\frac{\partial v_z}{\partial r}\right)^2\right] \tag{10}$$

where the turbulence model constants from refs [19, 20] are found in the following list: ($C_\mu = 0.09$, $C_1 = 1.44$, $C_2 = 1.92$, $\sigma_k = 1.0$, $\sigma_\varepsilon = 1.3$). The turbulent eddy viscosity is computed using the following expression:

$$\nu_t = \frac{\mu_t}{\rho} = C_\mu f_\mu \frac{k^2}{\varepsilon}\mathrm{e}^{-BN} \tag{11}$$

where $f_2 = \exp(-2.5/(1+R_T/50))$ and $f_\mu = (1.0 - 0.3\exp(-R_T^2))$ are the standard damping functions with ($R_T = \rho k^2/\varepsilon\mu$), Jones and Launder [20]. The equation for turbulent thermal conductivity is given by

$$K_t = \rho C \frac{\nu_t}{Pr_t} \tag{12}$$

where Pr_t is the turbulent Prandtl number, here taken as $Pr_t = 0.9$. It should be remarked that the damping of the magnetic field is modeled by the last terms in equations (8) and (9). The damping terms were modeled by considering the work done by the fluctuating fluid motion against the restraining influence of the magnetic field. The exponential terms e^{-BN} was derived from a simple analysis of fluid motion in a transverse magnetic field, shown below, which models the effectiveness of the electromagnetic damping.

One of the principal difficulties of modeling the turbulent pipe flow with a transverse magnetic field is the strong radial and angular dependence of electromagnetic damping. This is caused by the simultaneous distortion and interaction of the induced magnetic field and the mean velocity field. This effect, commonly referred to as the Hartmann effect, flattens the velocity profile and induces a hydromagnetic boundary layer close to the wall with a high induced electric current density at the top and bottom of the pipe cross section, causing a radial and azimuthal dependence in the problem.

The damping force within the Hartmann layer at the top and bottom of the pipe cross section is much higher than at the side region due to the high local electric current density. An angular and radial variation of the electromagnetic damping force can be evaluated by calculating the ratio of induced magnetic field gradients in the core region and in the region near the wall. The characteristic damping force in the core region is $|(\mathbf{j}\times\mathbf{B})|_c \sim \sigma \bar{v}_z B_0^2$, but due to higher mean induced electric current density, the characteristic damping force is higher within the Hartmann layer. Since the net electric current density across a vertical diameter is zero and the Hartmann layer is relatively small, the damping force in the Hartmann layer should go like the ratio of the pipe radius to the thickness of the hydromagnetic boundary layer,

$$|(\mathbf{j}\times\mathbf{B})|_H \sim \sigma \bar{v}_z B_0^2\left(\frac{R}{\delta_H}\right). \tag{13}$$

Therefore, the amplification of the electromagnetic damping within the Hartmann layer region can be estimated using the following expression:

$$D_m(r,\phi) = \frac{(\partial B_z/\partial y)_H}{(\partial B_z/\partial y)_C}. \tag{14}$$

This approximation is used since $j \sim \mu_0(\partial B_z/\partial y)$ and the gradient of the induced field was much simpler to evaluate than the local electric current density. Equation (14) naturally allows the calculation of the radial and angular variation of the electromagnetic damping force.

The presence of the exponential term (e^{-N}) in the electromagnetic damping model is obtained by considering motion of fluid in the transverse magnetic field. The time rate of change of fluid momentum is proportional to the force imposed by the transverse magnetic field and may be expressed by the following equation:

$$\rho\frac{\mathrm{d}u_\perp}{\mathrm{d}t} = -\sigma u_\perp B_0^2. \tag{15}$$

The solution of the deceleration of the fluid due to the damping influence of the transverse magnetic field is,

$$u_\perp(t) = u_{\perp,0}\,\mathrm{e}^{-t/t_m} \tag{16}$$

where ($t_m = \rho/\sigma B_0^2$) is the characteristic magnetic braking time.

The effectiveness of the turbulence damping process

depends on the ratio of the characteristic turbulent eddy turn-over time ($t_t = k/\varepsilon$) and t_m. The time scale for large energy containing eddies is ($t_t = L/\bar{v}_z$) and, hence, the ratio of these time scales gives,

$$\frac{t_t}{t_m} = \frac{\sigma B_0^2}{\rho}\left(\frac{k}{\varepsilon}\right)_{\text{large}} = \frac{\sigma B_0^2}{\rho}\frac{L}{\bar{v}_z} = N. \tag{17}$$

Comparing equations (16) and (17), the decay of velocity is

$$u_\perp(t_k) = u_{\perp,0}\, e^{-N} \tag{18}$$

and the average decay of the turbulent kinetic energy ($k \approx u^2$) is postulated to be proportional to e^{-N}. See ref. [21] for more details.

It should be remarked that the turbulence modeling approach results in an explicit coupling between the turbulence equations and the magnetic induction equation, and allows radial and angular variation of electromagnetic damping to be modeled with the equations. The principal advantage of this approach is that the abrupt change of electromagnetic damping within the Hartmann layer is automatically captured. No additional model for eddy viscosity or mixing length is needed and the model is easily incorporated into the k–ε turbulence model.

4. NUMERICAL SOLUTION OF GOVERNING EQUATIONS

The partial differential equations that describe the flow of liquid metal through a pipe with a transverse magnetic field are sufficiently complex that a numerical method must be employed to solve the governing equations. Here, an implicit and non-iterative space marching method developed by Patankar and Spalding [22] was used to solve the governing equations. The first step in obtaining the finite difference solution of the pipe flow equations is to overlay a suitable computational mesh over half of the pipe cross section using grid stretching using recommendations given by Thompson and Warsi [23], and replace the partial differential equations by a set of algebraic finite difference equations. The resulting set of algebraic equations is then solved iteratively to obtain a numerical solution to the partial differential equations.

5. RESULTS AND DISCUSSION OF RESULTS

The first step in the numerical analysis of the turbulent pipe flow with a transverse magnetic field was the validation of the numerical results for laminar flows in which the k–ε turbulence model is taken out of the picture. Computed velocity profiles and skin friction for laminar, isothermal MHD pipe flow were compared to the analytical solutions of Gold [7] and excellent results were obtained. Calculated local and average Nusselt numbers for the laminar MHD heat transfer problems showed good agreement with the analytical solutions of Gardner [24].

Turbulent flow validations were performed by initially assigning a power law velocity profile and setting turbulent kinetic energy and dissipation values using formulas suggested by Rodi and Scheuerer [25]. Hyperbolic tangent grid stretching was used in the radial direction with 50–80 grid points and 20 evenly spaced points in the azimuthal direction. The marching step size and the grid distribution was adjusted to ensure that skin friction computed from calculated axial pressure gradient matched the skin friction computed from velocity profiles. It was found that optimum results were obtained with y^+ between 1 and 2. The computations used 5000 marching steps or more to ensure complete convergence of the solution. Furthermore, for heat transfer calculations the step size was reduced until the imposed heat flux matched the calculated axial transport of thermal energy.

5.1. *Calibration of turbulence model: velocity profiles and skin friction*

The calibration of the k–ε turbulence model with electromagnetic damping terms was performed at $Re = 16\,000$, $Re = 50\,000$ and $Re = 150\,000$; and Hartmann number from 0 to 375. This was accomplished by comparing calculated velocity profiles and skin friction to the experimental data of ref. [8]. The Hartmann layer was modeled by coupling the turbulence equations with the magnetic induction equation via equation (14). It was found that the constants $A = 0.05$ and $B = 0.9$ produced optimum results.

Figures 3 and 4 show a comparison of computed velocity profiles with experimental data at 0, 45 and 90°. It can be seen that flattening of the velocity profile at 0° and the rounding of the velocity profile at 90° was correctly predicted by the turbulence model with the electromagnetic damping term. Although not shown, the original k–ε turbulence model was incapable of predicting the rounding of velocity profile at 90° because it lacks a term modeling the damping of turbulence by the magnetic field.

Figure 5 shows a comparison of computed skin friction with experimental data. It can be seen that the average skin friction was accurately predicted in the turbulent flow regime. For high Hartmann numbers, the flow is laminar and the curve fit of calculated skin friction closely matches the experimental data and Shercliff's analytical solution for laminar pipe flow with transverse magnetic field, [26]. These results showed that the turbulence model was capable of predicting the flow characteristics even when the turbulent fluctuations are damped out.

5.2. *Damping of turbulence*

The numerical predictions qualitatively show the turbulence suppression by the magnetic field. Figure 6 shows a set of typical contours of constant turbulent kinetic energy for flow at $Re = 50\,000$ and M from 23 to 91. Strong preferential damping at the top and bottom of the pipe can be seen. As the Hartmann

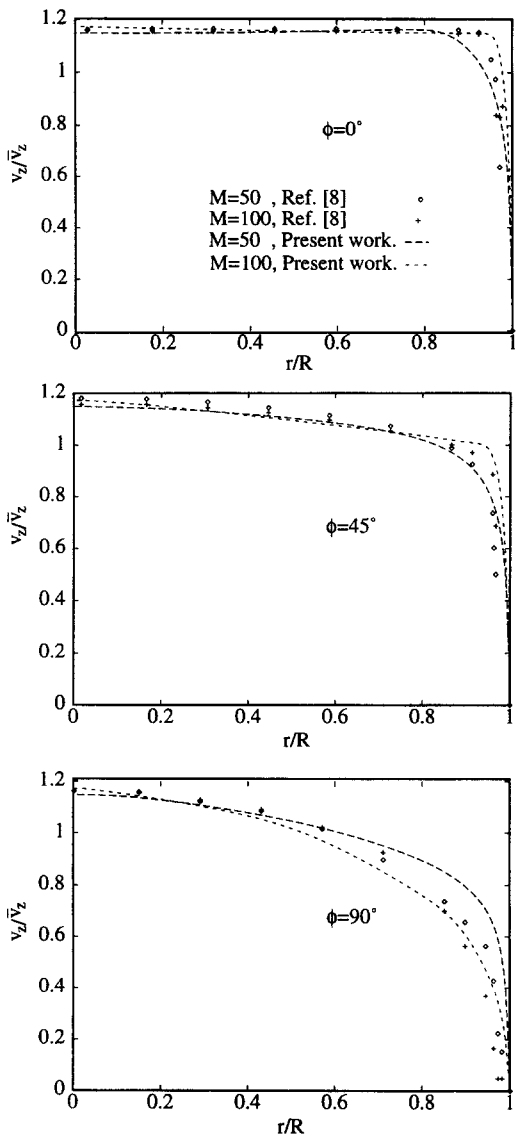

Fig. 3. Comparison of velocity profiles for $Re = 50\,000$.

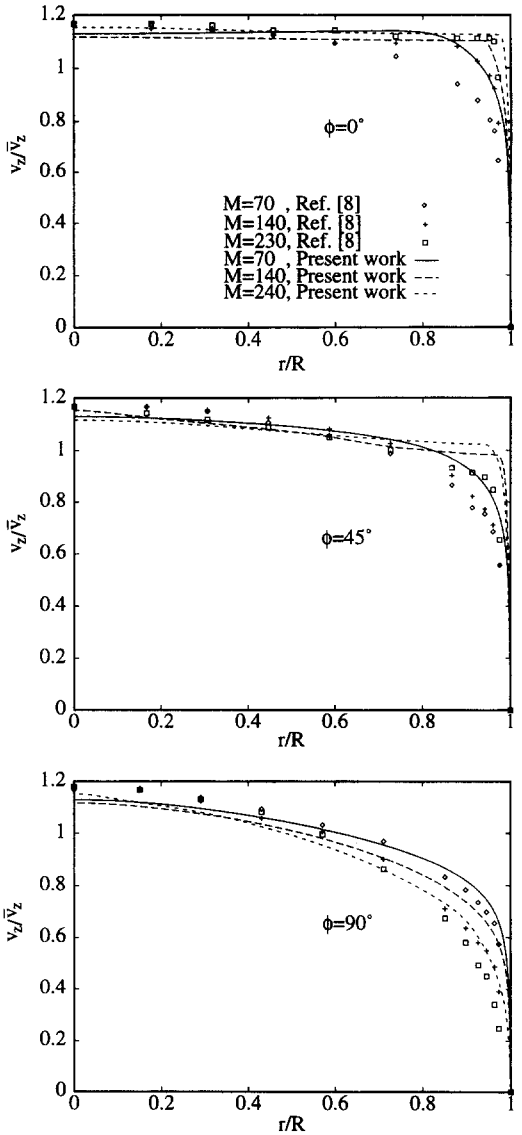

Fig. 4. Comparison of velocity profiles for $Re = 150\,000$.

number is increased, the turbulence at the side is the strongest, and the contour profiles suggest that there is a diffusion of turbulence from the side to top, bottom and center of the pipe. This damping behavior is consistent with measurements recorded by Patrick [9], Fig. 2, which indicate that turbulence at the side is the last region to be suppressed by the transverse magnetic field. It should be noted that similar turbulent kinetic energy contours were obtained at other Reynolds numbers.

In ref. [8] the profiles of axial turbulence intensity, T.I. $= \sqrt{v_z'^2}/\bar{v}_z$, was measured at several Reynolds numbers. By assuming that the radial and azimuthal fluctuations are equal to the axial fluctuations, those data were converted to an equivalent turbulent kinetic energy, $3/2(\text{T.I.})^2(\bar{v}_z^2)$, for comparison to the calculated turbulent kinetic energy of the present work. Figures 7 and 8 show this qualitative comparison of the converted data of ref. [8] and the computed turbulent kinetic energy of the present work. It can be seen that agreement between the calculated turbulent kinetic energy and the axial intensity is reasonable. The turbulence near the top of the pipe, and in particular in the core region, is damped quickly and this behavior is captured by the turbulence model. The turbulence near the wall does not die out as quickly due to the increased turbulence production caused by the steeping of the velocity profile caused by the Hartmann effect.

The damping of turbulence at the sides appear to be underpredicted by the k–ε turbulence model. The electromagnetic damping of turbulent fluctuations is anisotropic and the axial velocity fluctuations are preferentially damped by the transverse magnetic field. Consequently, the turbulence intensity estimated using the axial velocity fluctuation data results in a low estimate of the turbulent kinetic energy of the flow. It should be noted that for $\phi = 90°$, in particular,

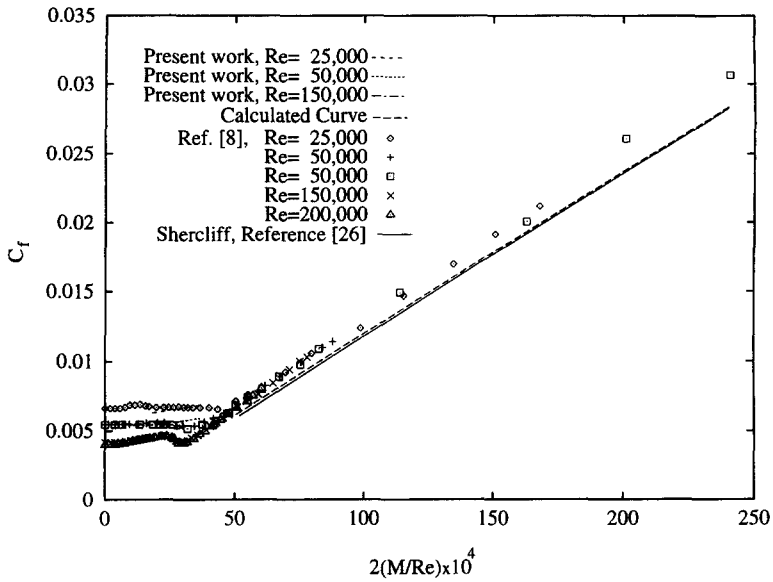

Fig. 5. Comparison of average skin friction data.

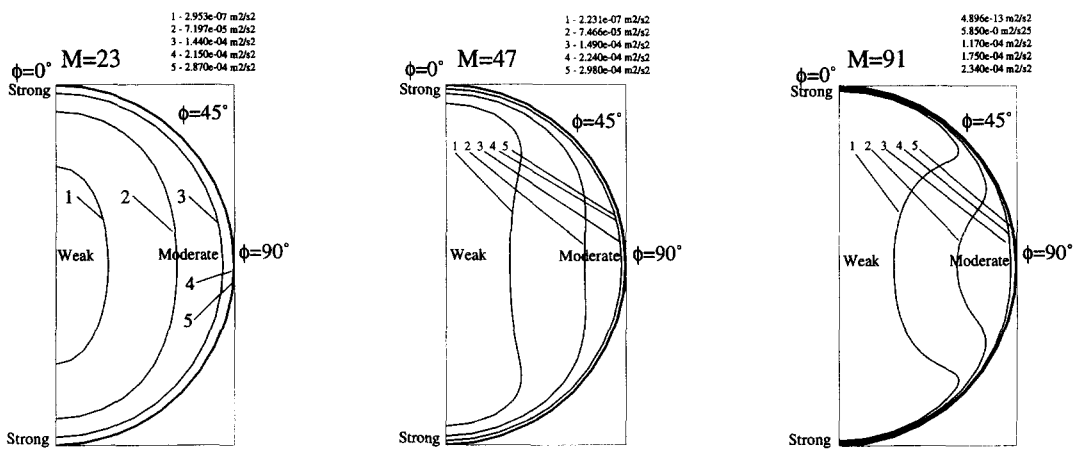

Fig. 6. Computed turbulent kinetic energy contours for $Re = 50\,000$.

the turbulent kinetic energy levels out at high M values. It is believed this leveling out is a result of the turbulent fluctuations aligning in the direction of the applied magnetic field which makes the damping of the turbulent velocity fluctuations less effective at higher M.

5.3. *Turbulent heat transfer and transverse magnetic field*

The heat transfer in a horizontal pipe with transverse magnetic field was modeled by employing the modified k–ε turbulence model. The heat transfer calculations were performed with the empirical constants A and B set to 0.05 and 0.9, respectively, and these constants were not adjusted anytime respectively for all calculations. It was reasoned that if the turbulence model was correctly formulated, it should also quantitatively predict the heat transfer process. Therefore, the heat transfer calculations were also used as means of validating the turbulence model.

In Fig. 9 the calculated turbulent Nusselt number was compared to correlation curves suggested by Lykoudis and Touloukian [27], Skupinski *et al.* [28] and Lubarsky and Kaufman [29]. It was found that the Nusselt number was moderately underpredicted using the k–ε turbulence model (10–20%) but the results were reasonable if one considers the limits of experimental uncertainty in the data used to determine the other correlations.

The heat transfer calculations with the electromagnetic damping model are given in Fig. 10 which shows a comparison of local Nusselt number at $\phi = 0$, 30, 60 and 90°. These results were obtained for $Re = 25\,000$–$1\,000\,000$; and M from 0 to 375. The accuracy of the solution appears to progressively improve from 0 to 90°. The agreement is better at Reynolds numbers above 100 000 and is best at the higher Hartmann number.

It should be noted the relatively poor accuracy at low Hartmann number is not surprising in view of the

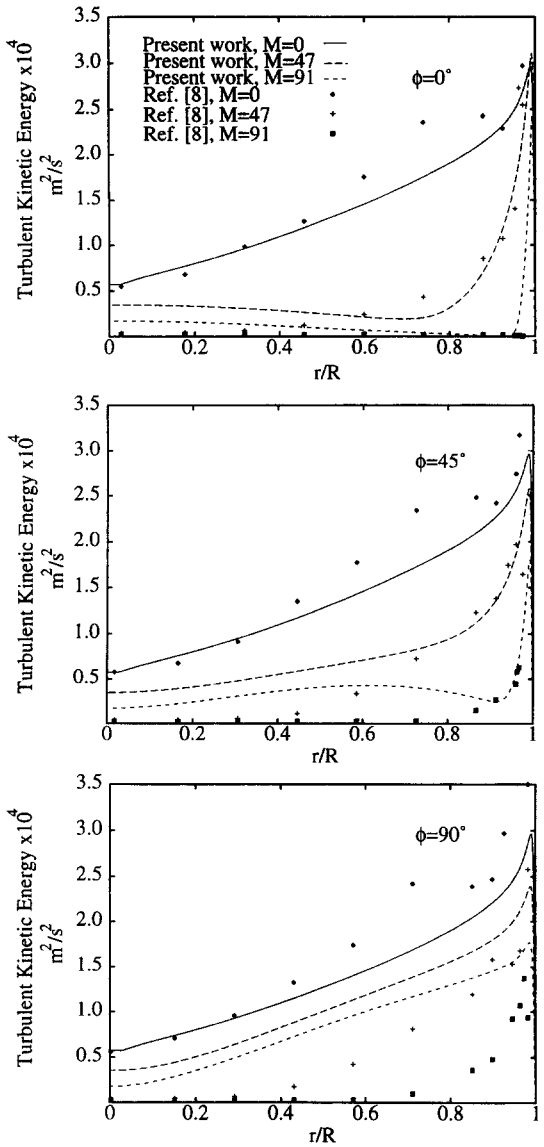

Fig. 7. Comparison of turbulence energy for $Re = 50\,000$.

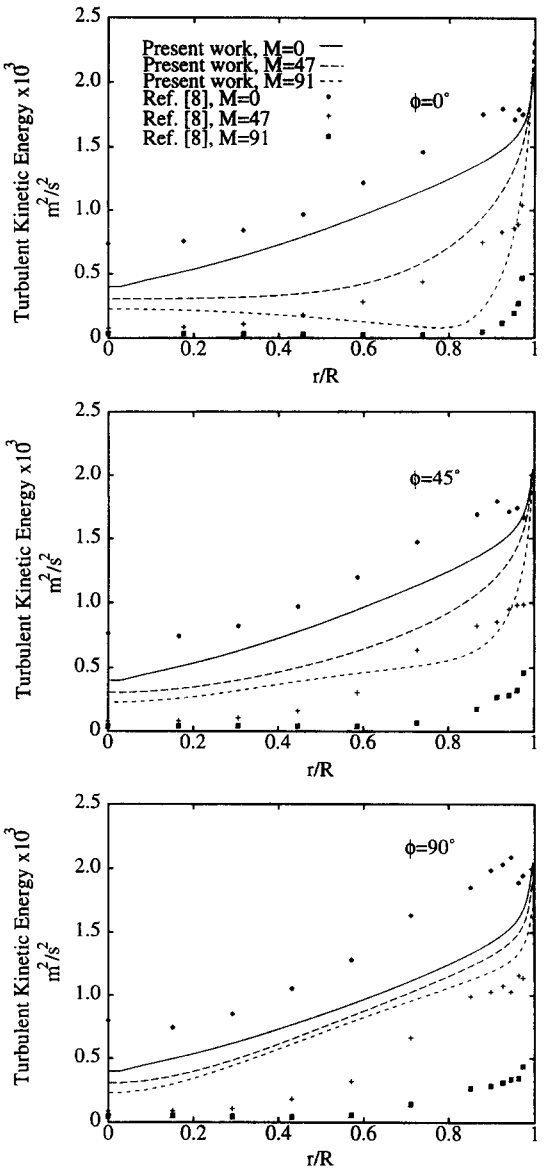

Fig. 8. Comparison of turbulence energy for $Re = 150\,000$.

fact that the original k–ε turbulence model underpredicted the average heat transfer coefficient for ordinary turbulent flow. However, good accuracy at high Reynolds number and Hartmann numbers are encouraging in view of the fact that the electromagnetic damping model was originally calibrated at much lower Reynolds and Hartmann numbers using only velocity profiles and skin friction data.

Examination of Fig. 10 indicates that the experimental data for the Nusselt number profiles crosses over at low Reynolds number and this behavior was correctly captured by the turbulence model. This crossover occurs because increase of heat transfer at the top from the steepening velocity profile exceeds the decrease of heat transfer brought on by the damping of turbulence by the magnetic field. The steepening of the velocity profile does not occur at other angles and the crossover behavior is consequently not observed at $\phi = 30$, 60 and 90°. It should be noted that the relatively poor agreement with the experimental data at Reynolds numbers less than 100 000 and angles less than 30° was caused by the natural convection present in the experimental data [13].

5.4. *Interaction of natural convection and transverse magnetic field*

In ref. [13] the authors indicated that their experimental temperature profiles demonstrated that natural convection was present and appeared to be significant under certain conditions. A limited number of calculations were performed including radial and azimuthal momentum equations, with the appropriate radial and angular buoyancy forces, in the set of equations to be solved simultaneously. The complexity of the numerical solution increased accordingly but it

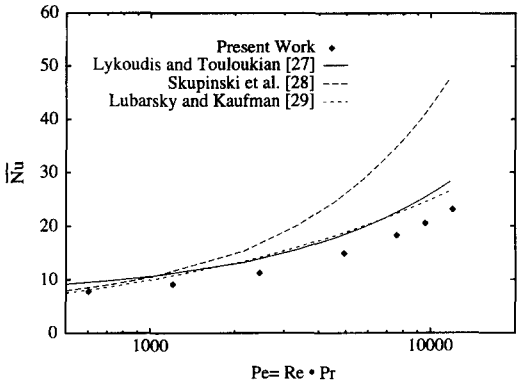

Fig. 9. Comparison of average Nusselt number for $M = 0$.

was necessary in order to assess the importance of natural convection.

With the buoyancy effects included in the equations, better agreement with the temperature profile data of ref. [13] was obtained. The computed temperature profiles were non-symmetric (except for $\phi = 90°$) as shown in Figs. 11–13 due to the secondary flow of the natural convection. It should be noted that the temperature profiles became progressively more symmetrical as increases in the transverse magnetic field suppressed more of the natural convection motion.

For $Re = 300\,000$ as shown in Fig. 13, there was not much advantage to be gained by modeling the natural convection since the nearly symmetric temperature profiles indicate that effect of natural convection is almost insignificant. It was found that there was practically no difference in the temperature profiles with or without the inclusion of the natural convection terms in the momentum equations. Also, there was not much difference in the average Nusselt number. These results suggest that natural convection may be safely omitted without incurring significant degradation in the accuracy of the computed results, particularly for high Reynolds numbers and high Hartmann numbers.

5.5. *Average Nusselt number*

Often, the average Nusselt number behavior is of primary interest. Figure 14 shows the calculated average Nusselt number as a function of the Peclet number and the Hartmann number. The average Nusselt number behavior shows the mutual antagonism of the inertial force and the magnetic force. At a fixed value of Reynolds number, increasing the Hartmann number results in a decrease in the Nusselt number, and for a fixed Hartmann number the Nusselt number curve approaches the ordinary turbulent pipe flow curve (i.e. $B_0 = 0$) as the Reynolds number is increased. The results of turbulent heat transfer cal-

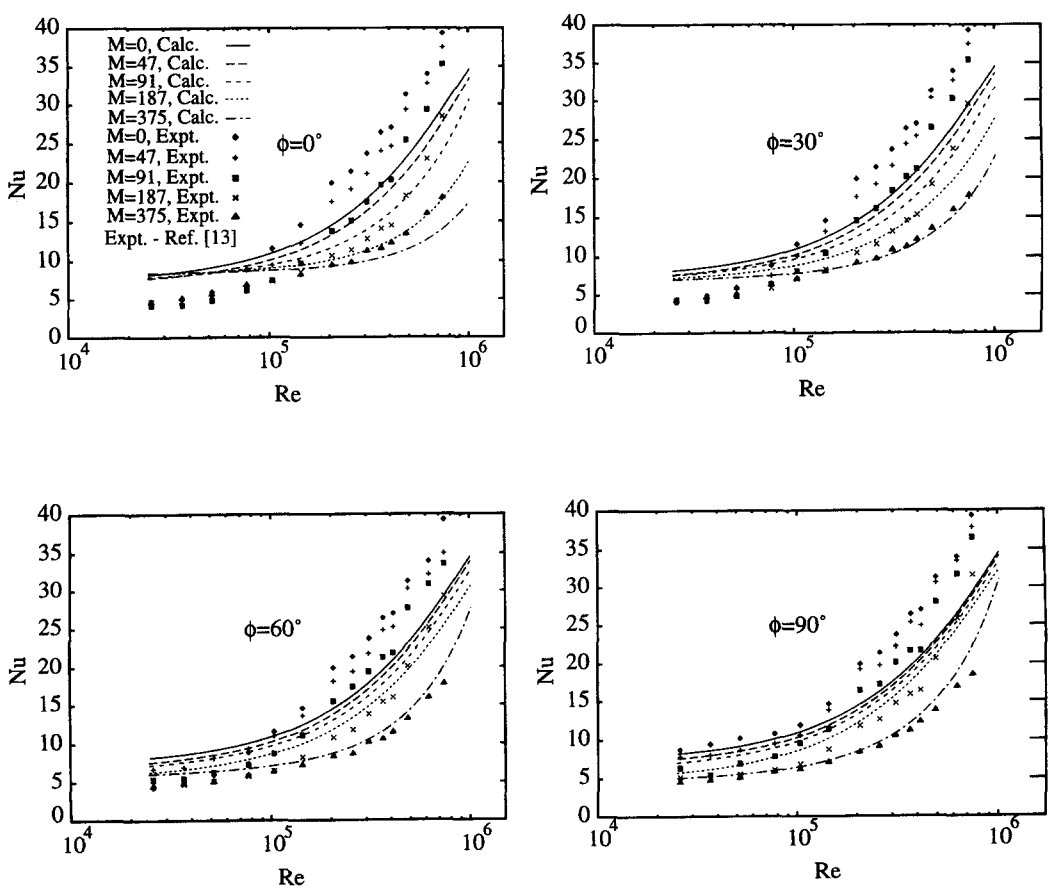

Fig. 10. Comparison of local Nusselt numbers.

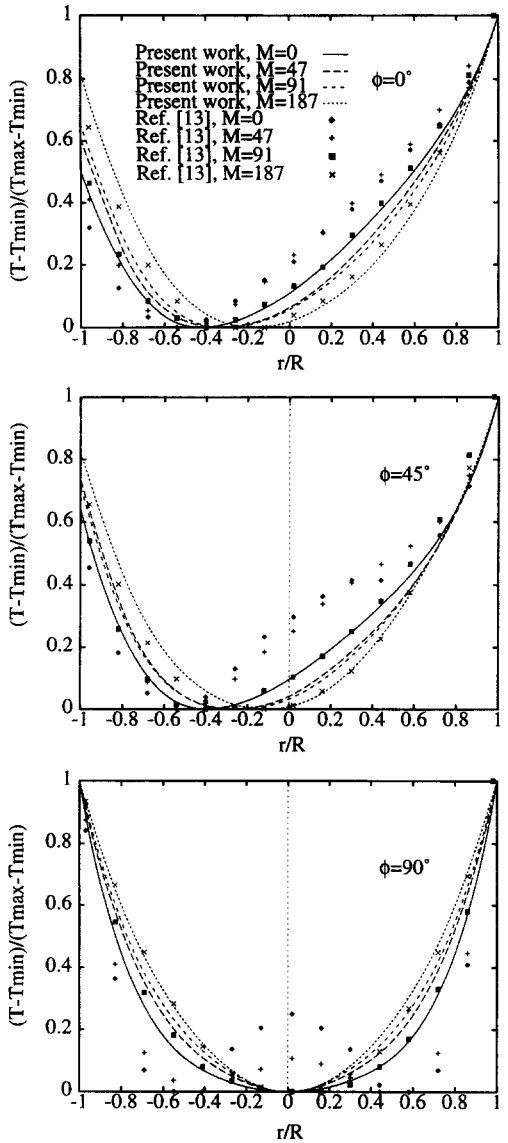

Fig. 11. Comparison of temperature profiles showing the effect of natural convection for $Re = 50\,000$, $Gr = 1.3 \times 10^7$.

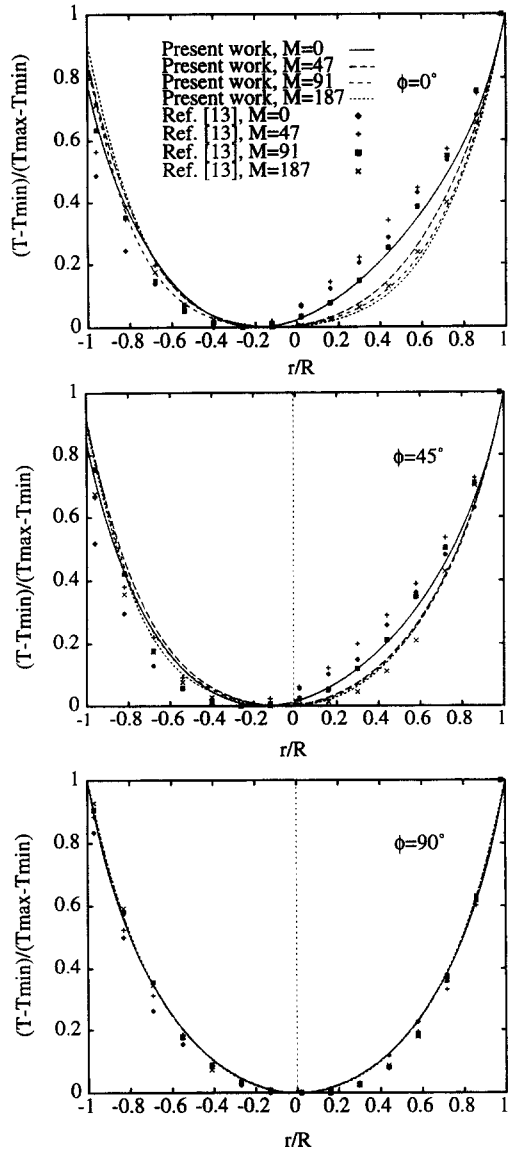

Fig. 12. Comparison of temperature profiles showing the effect of natural convection for $Re = 105\,000$, $Gr = 2.6 \times 10^7$.

culations may be summarized by a curve fit equation representing the average Nusselt number as function of the Peclet number and the Hartmann number,

$$Nu = 7 + \frac{0.00782 Pe^{0.811}}{[1 + 0.0004 M^{1.5} f(Pe)]}$$

where

$$f(Pe) = (0.3 + 4.75 \times 10^{-5} Pe - 2.10 \times 10^{-9} Pe^2). \quad (19)$$

It should be noted that the effect of natural convection on the average Nusselt number was systematically investigated for $Gr = 0$–10^7, and Re from 50 000 to 150 000. It was found that computations with natural convection did not appreciably change the average Nusselt number, even though natural convection caused some skewness in the temperature and velocity profiles. Consequently, equation (19) is a reasonable estimate of average Nusselt number for turbulent pipe flow with transverse magnetic field.

6. CONCLUSIONS

An electromagnetic damping model was formulated and incorporated into the k–ε turbulence model. The inclusion of radial and angular variation of electromagnetic damping was achieved by closely coupling the magnetic induction equation and turbulence equations. The turbulence model qualitatively showed the turbulence suppression by the magnetic field which was consistent with experimental observations noted in the literature. The computed velocity profile, skin friction, heat transfer and temperature profiles closely

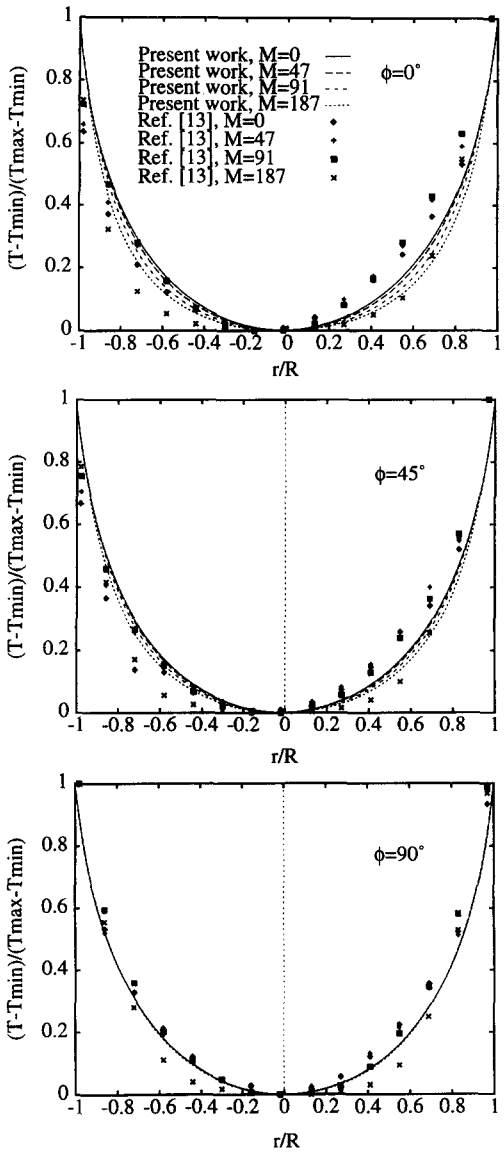

Fig. 13. Comparison of temperature profiles showing the diminishing effect of natural convection for $Re = 300\,000$, $Gr = 7.5 \times 10^7$.

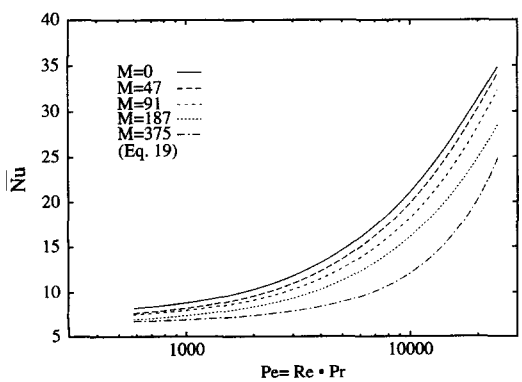

Fig. 14. Average Nusselt number with transverse magnetic field from equation (19).

matched the available experimental data. It is concluded that the turbulence model correctly modeled the electromagnetic damping of turbulence, and the encouraging results suggest that k–ε turbulence model can be adapted to model complex magnetohydrodynamic flows.

REFERENCES

1. Szekely, J. and Ilegbusi, O. J., *The Physical and Mathematical Modeling of Tundish Operations*. Springer, Berlin, 1989.
2. Branover, H. and Unger, Y., eds, Metallurgical technologies, energy conversion, and magnetohydro magnetic flows. *Progress in Astronautics and Aeronautics*, 1993, **148**.
3. Imaichi, K. The superconducting magnetohydrodynamic propulsion system of Yamato-1 : design, structure and performance. A preprint available from The Institute of Marine Engineers, The Memorial Building, 76 Mark Lane, London EC3R 7JN, 1992.
4. Branover, H. and Unger, Y., eds, Advances in turbulence studies. *Progress in Astronautics and Aeronautics*, 1993, **149**.
5. Bradshaw, P. Collaborative testing of turbulence models. Final Report on AFOSR 90-154, Air Force Office of Scientific Research, Bldg. 410, Bolling AFB, DC 20332-6448, 1992.
6. Ferraro, V. C. A. and Plumpton, C., *Magneto-Fluid Mechanics*. Clarendon Press, Oxford, 1966.
7. Gold, R. R., Magnetohydrodynamic pipe flow. Part 1. *Journal of Fluid Mechanics*, 1962, **13**, 505.
8. Gardner, R. A. and Lykoudis, P. S., Magneto-fluid-mechanic pipe flow in a transverse magnetic field Part 1. Isothermal flow. *Journal of Fluid Mechanics*, 1971, **47**, 737–764.
9. Patrick, R. P., Magneto fluid mechanic turbulence. Ph.D. thesis, Purdue University, Lafayette, Indiana, 1971.
10. Genin, L. G., Manchkha, S. P. and Sviridov, V. G., Effect of longitudinal magnetic field on profiles of temperature, heat transfer, and turbulent heat transfer. *Magnitnaya Gidrodinamika*, 1974, **1**, 70–77.
11. Genin, L. G., Kovalev, S. I. and Sviridov, V. G., Convective heat transfer for a liquid metal in a pipe in a longitudinal magnetic field. *Magnitnaya Gidrodinamika*, 1987, **4**, 31–36.
12. Gardner, R. A. and Lykoudis, P. S., Magneto-fluid mechanic pipe flow in a transverse magnetic field with and without heat transfer. AIAA Paper no. 69-723, 1969.
13. Gardner, R. A. and Lykoudis, P. S., Magneto-fluid mechanic pipe flow in a transverse magnetic field part 2. Heat transfer. *Journal of Fluid Mechanics*, 1971, **48**, 129–141.
14. Branover, G. G., Construction of a unique semiempirical theory of turbulent flow in tubes in a magnetic field. *Magnitnaya Gidrodinamika*, 1968, **4**(3), 3.
15. Branover, G. G. and Vasil'ev, A. S., Turbulent flow in a plane perpendicular to a magnetic field. *Magnitnaya Gidrodinamika*, 1969, **5**(2), 47–49.
16. Branover, G. G. and Gel'fgat, Y. M., Turbulent Hartmann flow between rough walls. *Magnitnaya Gidrodinamika*, 1969, **4**(4), 42.
17. Branover, G. G., Gel'fgat, Y. M. and Tsinober, A. B., Turbulent magnetohydrodynamic flows in prismatic and cylindrical ducts. *Magnitnaya Gidrodinamika*, 1966, **2**(3), 1–12.
18. Lykoudis, P. S. and Brouillette, E. C., Magneto-fluid-mechanic channel flow. II. Theory. *Physics of Fluids*, 1966, **10**, 1002.
19. Launder, B. E., Morse, A., Rodi, W. and Spalding, D. B., A comparison of six turbulence models. NASA Con-

ference on Free Shear Flows, Langly, Hampton, Virginia, 1972.
20. Jones, W. P. and Launder, B. E., The calculation of low-Reynolds number phenomena with two-equation model of turbulence. *International Journal of Heat and Mass Transfer*, 1973, **16**, 1119–1130.
21. Ji, Hyun Chul, Analysis of turbulent pipe flow with transverse magnetic field. D.Sc. thesis, Washington University, St. Louis, Missouri, 1994.
22. Patankar, S. V. and Spalding, D. B., A calculation procedure for heat, mass and momentum heat transfer in three-dimensional parabolic flows. *International Journal of Heat and Mass Transfer*, 1971, **15**, 1787–1806.
23. Thompson, J. F., Warsi, Z. U. A. and Mastin, C. W., Numerical grid generation. Foundations and applications. North Holland, Amsterdam, 1985.
24. Gardner, R. A., Laminar pipe flow in a transverse magnetic field with heat transfer. *International Journal of Heat and Mass Transfer*, 1968, **11**, 1076–1081.
25. Rodi, W. and Scheuerer, S., Calculation of laminar-turbulence boundary layer transition on turbine blades. In *Proceedings of the 65th AGARD-REP Symposium on Heat Transfer and Cooling on Gas Turbines*, Bergen, Norway, 1985, pp. 18-1–8-2.
26. Shercliff, J., Determination des coefficients de convection d'un alliage sodium potassium dans un tube circulaire. *Journal of Fluid Mechanics*, 1956, **1**, 644.
27. Lykoudis, P. S. and Touloukian, Y. S., Heat transfer in liquid metals. *Transactions of the ASME*, 1958, 653–666.
28. Skupinski, E. S., Turtel, J. and Vautrey, L., The flow of conducting fluids in circular pipes under transverse magnetic field. *International Journal of Heat and Mass Transfer*, 1965, **8**, 937.
29. Lubarsky, B. and Kaufman, S. J., Review of experimental investigation of liquid metal heat transfer. NACA Technical Note 3336, 1955.